Scientific Research Publishing

Journal of Electromagnetic Analysis and Applications, 2026, 18(11), 217-230
https://www.scirp.org/journal/jemaa
ISSN Online: 1942-0749
ISSN Print: 1942-0730

Amplification of Terahertz Optical Phonons and Plasmons by 2D Electron Drift in the Structures Graphene-Semiconductor and in Heterostructures

Volodymyr Grimalsky[1], Margarita Tecpoyotl-Torres[1], Yuriy Rapoport[2], Oskar Nava-Fuerte[1]

[1]Center for Investigations on Engineering and Applied Science (CIICAp), Institute for Investigations on Basic and Applied Science (IICBA), Autonomous University of State Morelos (UAEM), Cuernavaca, Mexico
[2]Space Radio-Diagnostic Research Centre, University of Warmia and Mazury (UWM), Olsztyn, Poland
Email: v_grim@hotmail.com, tecpoyotl@uaem.mx, oskar.nava@uaem.edu.mx, yuriy.rapoport@gmail.com

How to cite this paper: Grimalsky, V., Tecpoyotl-Torres, M., Rapoport, Y. and Nava-Fuerte, O. (2026) Amplification of Terahertz Optical Phonons and Plasmons by 2D Electron Drift in the Structures Graphene-Semiconductor and in Heterostructures. *Journal of Electromagnetic Analysis and Applications*, **18**, 217-230.
https://doi.org/10.4236/jemaa.2026.1811011

Received: September 1, 2026
Accepted: October 31, 2026
Published: November 3, 2026

Copyright © 2026 by author(s) and Scientific Research Publishing Inc.
This work is licensed under the Creative Commons Attribution International License (CC BY 4.0).
http://creativecommons.org/licenses/by/4.0/

Open Access

Abstract

Generation and amplification of terahertz oscillations is investigated theoretically in structures graphene-semiconductor layers. The instability of hybrid space charge waves in graphene-optical phonons or plasmons in semiconductor layers is of Cherenkov type. It can be realized when the drift velocity of 2D electron gas in graphene exceeds some critical value. The numerical simulations of instability are based on the quantum kinetic approach. The main obstacle of implementing the specified instability is the heating of 2D electron gas during its drift. Therefore, the investigations are performed for moderately low temperatures $T \leq 200$ K, and the electron gas is degenerated. The best results are obtained for the structures with nitride semiconductors GaN, InN, A comparison with the drift instability in semiconductor heterostructures with 2D electron gas is given too, where the increments of instability are comparable.

Keywords

Graphene, Nitride Semiconductors, 2D Electron Drift, Terahertz Hybrid Waves, Instability

1. Introduction

Terahertz (THz) oscillations and waves [1]-[9] are used for transmitting information with increased information capacity, spectroscopy, intravision, radars etc. There are various methods of generation of THz radiation that are like optical

ones. They are antennas excited by short laser pulses, quantum cascade lasers, lasers on cyanides, and optical mixing [2] [6] [10]. Also, there are methods of generation of THz oscillations that are used earlier in microwaves and millimeter wave techniques. They are diode generators, transistors, vacuum tube devices, and frequency multipliers [3] [8] [9]. An important scientific and practical problem is the development of physical foundations of technologies for generating and amplifying THz oscillations with miniature and planar meta- and nanophotonic structures.

From various methods for generating THz oscillations in planar graphene-dielectric or graphene-semiconductor structures, in this paper the generation is chosen by a drift of 2D electron gas ш the graphene [11]-[13], since this scheme is quite simple and easily tunable. The mechanism is Cherenkov one [14]; it is like one used in travelling wave tubes and occurs when the drift velocity exceeds a critical value. The parameters of the generated THz oscillations can be effectively controlled by external electric and/or magnetic fields. As a preliminary result, either non-doped polar semiconductors, like *i*-GaAs, or nonpolar ones, like *n*-Si, were considered [13]. The joint action of optical phonons and plasmons in semiconductors was not investigated there.

Still there is a problem of choosing semiconductors to get the maximum increments of generation of THz oscillations in the structures graphene-semiconductor. As perspective materials, polar nitrides GaN, InN may be considered, where not only more efficient excitation of optical phonons may occur, but also the electron concentrations due to doping can be higher than in *n*-GaAs. A possible increasing increment of the drift instability under joint action of optical phonons and plasmons is of interest. A comparison with the drift instability in heterostructures with quantum wells on the base of nitrides also should be made.

The goal of the work is to select and justify a promising method for generating and processing THz signals based on the physics of nanostructures. The geometry of the problem is presented in **Figure 1**. There occurs the instability or amplification of coupled, or hybrid, space charge waves (SCW) in graphene-optical phonons and plasmons in surrounding semiconductor layers. This instability is of a Cherenkov type, so it can be realized at 2D electron drift velocities in the graphene, which are higher than some threshold value. The graphene sheet is in $z = 0$, it is surrounded by semiconductors or polar dielectric layers. The semiconductor layers can be either undoped or doped; in the last case the electronic plasmons can be excited. If a doped semiconductor is polar, then the excitation of coupled optical phonons and electron plasmons occurs.

Earlier it was investigated [12] [13] the instability of hybrid SCW-optical phonons due to drift of 2D electron gas in polar semiconductor heterostructures. It was assumed that the heterostructure is selectively doped and all the electrons are localized in the quantum channel. Thus, only optical phonons interacted with the drifting 2D electron gas. Two methods were applied to consider the dynamics of 2D electron gas, hydrodynamic and kinetic ones. The best results were obtained

for the quantum structures based on GaAs, compared to ones on the base of InSb or InAs. The increments of instability computed from the kinetic approach were smaller than ones from the hydrodynamic approach, but they were quite high for experimental observations. In the present paper the main attention is given namely to the quantum kinetic approach [12]-[18] for the structures with graphene and comparison with the instability in heterostructures with the drift of 2D electron gas.

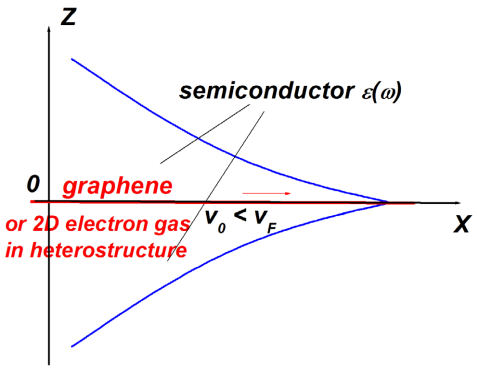


Figure 1. Geometry of the problem. Amplification of surface hybrid SCW in the structure graphene-semiconductor or heterostructure-semiconductor takes place by the drift of 2D electron gas in graphene or in a quantum channel within a heterostructure. The hybrid wave propagates along OX axis. Along OY axis the system is uniform.

2. Basic Equations

The basic equations are one for the density matrix for the motion of 2D electronic gas in graphene [15] [16] [18], or equivalently for the Wigner distribution function $f(\boldsymbol{p},\boldsymbol{r},t)$, and the quasi-stationary Poisson equation for the variable electric potential $\tilde{\varphi}$ in a bulky semiconductor, SI units:

$$\Delta\tilde{\varphi} = -\frac{e}{\varepsilon_0\varepsilon(\omega)}\tilde{n}_2\cdot\delta(z);\ \tilde{n}_2 = \frac{4}{4\pi^2}\int\int_{-\infty}^{\infty}\tilde{f}(\boldsymbol{p})\mathrm{d}p_x\mathrm{d}p_y. \tag{1}$$

here $\tilde{n}_2$ is the variable part of 2D electron concentration in graphene, $\varepsilon(\omega)$ is the effective permittivity in semiconductor layers, $\tilde{f}$ is the variable part of the distribution function. The hybrid space charge wave in graphene-optical phonons and plasmons in semiconductor layers are localized along OZ axis and propagate in x-direction.

The distribution function is searched as:

$$f \equiv f_0(\boldsymbol{p}) + \left(\tilde{f}(\boldsymbol{p})\exp(-\mathrm{i}\omega t + ikx) + c.c.\right);\ \tilde{n}_2, \tilde{\varphi} \sim \exp(-\mathrm{i}\omega t + ikx). \tag{2}$$

here the longitudinal wave number k is real, the frequency ω is complex, $\omega \equiv \omega' + \mathrm{i}\omega''$. Namely the simulations of the increment of instability $\omega'' > 0$ are the most interesting. Along OY axis the structure is uniform. The quasi-stationary approximation can be applied because of slow phase velocities of hybrid waves, $\omega'/k \ll c$.

Due to 2D electron drift, the steady part of the distribution function f_0 is the shifted Fermi one:

$$f_0(\boldsymbol{p}) = \left\{1+\exp\left[\frac{\left(\left(p_x-p_0\right)^2+p_y^2+p_g^2\right)^{1/2}-p_F}{p_T}\right]\right\}^{-1};$$
$$\boldsymbol{p}\equiv\left(p_x,p_y\right);\ \boldsymbol{k}\equiv(k,0);\ p_F\equiv\frac{E_F}{\hbar v_F};\ p_T\equiv\frac{k_BT}{\hbar v_F}. \tag{3}$$

here E_F is the Fermi energy in graphene, $v_F = 10^8$ cm/s is the Fermi velocity there, T is the electron temperature in Kelvins.

The recent theoretical and experimental results demonstrated that in graphene the electron-electron collisions dominate over electron-lattice ones [19]-[21] under the values of 2D electron concentration $n_{20} \approx 10^{12}$ cm^{-2}. This validates the representation Equation (2) for the distribution function. Also, for the graphene the hydrodynamic approach was confirmed in [21].

The value of the electron wave number p_0 due to the nonzero drift velocity has been computed from the nonlinear dependence of the density of the electron current on the bias electric field [17]:

$$n_{20}v_0 = \frac{1}{\pi^2}\int_{-\infty}^{\infty}\int v_x f_0(\boldsymbol{p})\mathrm{d}p_x\mathrm{d}p_y;\ \overline{v}\equiv\frac{1}{\hbar}\frac{\partial E}{\partial\overline{p}}. \tag{4}$$

here $v_0 < v_F$ is the corresponding value of the drift velocity of 2D electron gas. The equilibrium 2D electron concentration in graphene is n_{20}, $n_{20} = 10^{11}$ - 10^{12} cm^{-2} in the simulations. The dependence of the electron energy in graphene E on the electron wave vector $\boldsymbol{p}$ is [22] [23]:

$$E^2 = \hbar^2v_F^2\cdot\left(p^2+p_g^2\right);\ p_g\equiv\frac{m_g^*v_F}{\hbar};\ p^2\equiv p_x^2+p_y^2. \tag{5}$$

For the sake of generality, a small nonzero mass is included in graphene $m_g^* < 10^{-3}m_e$. In our simulations its influence is unessential when 2D electron concentration is $n_{20} \geq 3\times10^{11}$ cm^{-2}.

The equation for the variable part of the Wigner distribution function is [15] [16]:

$$\left[\hbar\cdot\left(\omega+i\nu_p\right)-E\left(\boldsymbol{p}+\frac{\boldsymbol{k}}{2}\right)+E\left(\boldsymbol{p}-\frac{\boldsymbol{k}}{2}\right)\right]\tilde{f}(\boldsymbol{p})$$
$$=-e\tilde{\varphi}(z=0)\cdot\left[f_0\left(\boldsymbol{p}-\frac{\boldsymbol{k}}{2}\right)-f_0\left(\boldsymbol{p}+\frac{\boldsymbol{k}}{2}\right)\right]. \tag{6}$$

The resulting dispersion equation for the amplified hybrid SCW is

$$\varepsilon(\omega)+Q(\omega,k)=0;$$
$$Q(\omega,k)\equiv\frac{e^2}{2\pi\varepsilon_0\hbar k}\frac{1}{\pi^2}\int_{-\infty}^{\infty}\int\frac{\left[f_0\left(\boldsymbol{p}+\frac{\boldsymbol{k}}{2}\right)-f_0\left(\boldsymbol{p}-\frac{\boldsymbol{k}}{2}\right)\right]}{\omega+i\nu_p-\frac{E\left(\boldsymbol{p}+\frac{\boldsymbol{k}}{2}\right)-E\left(\boldsymbol{p}-\frac{\boldsymbol{k}}{2}\right)}{\hbar}}\mathrm{d}p_x\mathrm{d}p_y. \tag{7}$$

here $\nu_p \approx (10^{12} \div 10^{13})$ s^{-1} is the electron collision frequency in graphene used in the equation for 2D electron gas there.

Equation (7) has been solved by iterations. Namely for the parameters used under simulations it is satisfied $\left|Q(\omega \cdot k)\right| < 0.5$ in Equation (7); this has been checked under simulations. Note that in simulations below the condition $\left|\omega''\right| \ll \omega'$ has been satisfied.

Changing variables have been applied, $p_x = p_0 + p \cdot \cos\theta$, $p_y = p \cdot \sin\theta$, *i.e.* the polar coordinate frame in the momentum space. For the integration with respect to p, the Landau rule should be satisfied [16], namely the contour of integration should be lower than all the poles. In the case of instability $\omega'' > 0$ the integration can be used along the real axis, *i.e.* p can be chosen as real. Because of relatively high values of electron collision frequency in the graphene, the integration can be realized as $0 \le p < +\infty$. To provide the integration over p, the subdivision into 2 regions has been done, $0 \le p \le p_1$ and $p_1 \le p < +\infty$. The value of p_1 has been chosen from the condition $k < p_1$, where k is the value of the wave number for the realization of instability. For the integration over the first region, the Simpson formula has been applied, for the second one it has been used the Gauss-Laguerre quadrature. The integration over θ, $0 \le \theta < 2\pi$, has been done by the Simpson formula [24].

The general case of doped semiconductors is considered. The dependence of the permittivity of the bulk semiconductor on frequency is [25]:

$$\varepsilon(\omega) = \varepsilon_\infty + \frac{(\varepsilon(0) - \varepsilon_\infty)\cdot\omega_T^2}{\omega_T^2 - \omega\cdot(\omega + i\gamma_1)} - \frac{\omega_{pV}^2}{\omega\cdot(\omega + i\gamma_2)};\ \omega_{pV}^2 \equiv \frac{e^2 n_0}{\varepsilon_0 m_V^*}. \tag{8}$$

here $\varepsilon(0)$, ε_∞ are the low- and high frequency lattice permittivities, ω_T is the frequency of transverse optical phonons, ω_{pV} is the volume plasma frequency, n_0 is the volume concentration in a semiconductor, m_V^* is the effective mass there; the parameters γ_1, γ_2 are the dielectric dissipation and electron collision frequency in a semiconductor, correspondingly.

The hybrid SCW-optical phonons or plasmons waves possess an instability near the resonant frequency, which is determined from the relation $\varepsilon(\omega) = 0$.

Thus, there is a possibility to manage the resonant frequencies in semiconductors due to variation of the plasma frequency under different doping levels. In the case of polar semiconductors like InSb, InAs, GaAs, GaN, and InN, both oscillations of the crystalline red, or optical phonons, and electron plasmons are important. In the non-polar semiconductors, like n-Si or n-Ge, only electron plasmons interact with SCW in graphene.

An alternative simpler approach to the dynamics of 2D electron gas is hydrodynamics [17] [19]. The nonzero "kinetic" effective mass $m^* = \hbar p_F / v_F$, $p_F \equiv (\pi n_{20})^{1/2}$ has been introduced in graphene [17], which was determined from the comparison of fully quantum kinetic and hydrodynamic approaches for the nonlinear dependence of 2D density of electron current on THz electric field. Under 2D electron concentrations $n_{20} = (3 \times 10^{11} \div 10^{12})$ cm^{-2} the "kinetic" effective masses are about $(0.01 \div 0.02)\, m_e$.

To compare with the structures graphene-semiconductor, also the instability of hybrid waves is considered in heterostructures with selective doping, where 2D

electron gas of high mobility is used within the quantum well. Because selective doping is used in the heterostructures, where almost all electrons are localized within the quantum channel, only the interaction with the optical phonons is considered there, *i.e.* the bulky semiconductor out of the quantum channel is completely depleted, $n_0 = 0$. The collision frequencies of 2D electron gas there can be essentially smaller than in graphene, $\nu_p \le 10^{11}\ \mathrm{s}^{-1}$ [10] [18].

Only the lowest quantum sub-level is considered in the quantum well. The dispersion equation for the electrons is:

$$E_\alpha(\boldsymbol{p}) = E_{\alpha 0} + \hbar^2 \frac{(p_x - p_{10})^2 + p_y^2}{2m_1^*};\ \ p_{10} \equiv \frac{m_1^* v_0}{\hbar}. \tag{9}$$

The steady part of the distribution function is generally Fermi, but it can be approximated by the step function:

$$\begin{aligned} &f_{10}(\boldsymbol{p}) \approx \theta\left(p_{F1}^2 - (p_x - p_{10})^2 - p_y^2\right); \\ &\theta(u) \equiv \begin{cases} 0, & u < 0; \\ 1, & u > 0. \end{cases} \end{aligned} \tag{10}$$

In Equation (10) the Fermi wave number is $p_{F1} \approx (2\pi n_{20})^{1/2}$; $E_{F1} \equiv E(p_{F1})$; $E_{\alpha 0} \equiv 0$. Within the quantum well, the electron energy is measured from the bottom of the lowest quantum sub-level.

The dispersion equation has been obtained from Equation (6) [11] [12], where the multiplier $1/2\pi^2$ is used instead of $1/\pi^2$, because of the presence of a single Γ-valley in GaAs, GaN, and InN [25] [26]:

$$\varepsilon(\omega) + \frac{e^2 m_1^*}{2\pi\varepsilon_0 \hbar^2 k^2} M_{11} \frac{1}{2\pi^2} \int\int_{-\infty}^{\infty} \frac{f_{10}\left(\boldsymbol{p} + \frac{\boldsymbol{k}}{2}\right) - f_{10}\left(\boldsymbol{p} - \frac{\boldsymbol{k}}{2}\right)}{\frac{m_1^*}{k\hbar}(\omega + i\nu_p) - p_x} \mathrm{d}p_x \mathrm{d}p_y = 0. \tag{11}$$

here $M_{11} \approx 1$ is the matrix element for the wave function $\psi_1(z)$ of the lowest quantum sub-level [11] [12] [15]:

$$M_{11} = \int_{-\infty}^{+\infty}\int_{-\infty}^{+\infty} \exp(-k|z - z'|)\psi_1^2(z)\psi_1^2(z')\mathrm{d}z\mathrm{d}z';\ \ \int_{-\infty}^{+\infty} \psi_1^2(z)\mathrm{d}z \equiv 1. \tag{12}$$

As already mentioned, in the heterostructures the electron collision frequencies are essentially smaller than ones in the graphene. Therefore, to satisfy the Landau rule and to provide accuracy of simulations, it has been necessary to integrate within the complex plane. For this purpose, the contour of integration for p_x has been subdivided into 3 parts. Two parts are along the real axis of p_x, from $-\infty$ to $-p_c$ and from p_c to $+\infty$. Here p_c should be bigger than the values of the wave number k where the instability has been realized. The central part is along the half-circle in the complex plane of p_x specifically, to provide the Landau rule, namely the possible poles should be located above the contour of integration. For the semi-infinite parts of the contour, the integration by means of the Gauss-Laguerre quadrature has been applied, whereas for the half-circle the Simpson one has been used. As in Equation (7), for typical parameters of the heterostructures the iterations can be

applied for Equation (11).

In the case of relatively low electron temperatures $T \leq 80$ K and high 2D electron concentrations $n_{20} \geq 3 \times 10^{11}$ cm^{-2}, the step-like approximation Equation (10) can be used, and integration in Equation (11) has been realized analytically [12] [15].

3. Simulations

The simulations of increments of instability $\omega'' \equiv \mathrm{Im}(\omega)$ have been realized for different parameters of graphene sheets and for different semiconductors. The realistic parameters of graphene and semiconductor layers have been used. In the simulations presented below 2D electron concentration in graphene is $n_{20} = 10^{12}$ cm^{-2}, the electron collision frequency is $\nu_p = 2 \times 10^{12}$ s^{-1} there, the electron temperatures are $T = (50 \div 200)$ K. Under these moderately low temperatures, the electron collision frequencies in doped semiconductors are low, $\gamma_1 = (2 \times 10^{12} \div 2 \times 10^{13})$ s^{-1}.

The electron drift velocities are moderate here, $v_0 \leq 0.6 v_F$, because at higher drift velocities the nonlinearity becomes essential. To get the instability under moderately high drift velocities, 2D concentrations should be quite high [13], $n_{20} \geq 5 \times 10^{11}$ cm^{-2}. The electron concentrations in bulk semiconductors are moderate, *i.e.* they do not exceed essentially the density of states in the conduction band N_c at the temperature $T = 300$ K, $n_0 \leq N_c \sim T^{3/2}$. Thus, the effects of narrowing forbidden gaps are not considered here.

For non-polar n-Si the lattice permittivities are equal, $\varepsilon(0) = \varepsilon_\infty = 11.9$, the electron effective mass is $m_v^* = 2 \times 10^{-31}$ kg, $N_c = 3.2 \times 0^{19}$ cm^{-3} at $T = 300$ K. The parameters of the polar semiconductor layers are given in **Table 1** [25] [26].

Table 1. The parameters of the polar semiconductor layers used in simulations.

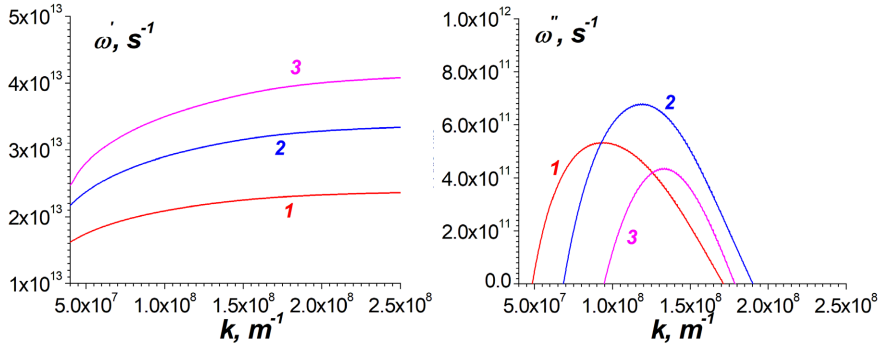
Semiconductor	Low-frequency lattice permttivity $\varepsilon(0)$	High-frequency lattice permttivity ε_∞	The frequency of transverse optical phonons ω_T, s^{-1}	The dielectric dissipation γ_1, s^{-1}	The electron effective mass m_v^*, kg	The density of states in the conduction band N_c, cm^{-3} ($T = 300$ K)
GaAs	12.9	10.9	5.1×10^{13}	4×10^{11}	6×10^{-32}	4.7×10^{17}
GaN, zinc blende	9.7	5.3	1.04×10^{14}	5×10^{11}	1×10^{-31}	1.2×10^{18}
InN, wurtzite	14.0	5.8	8.48×10^{13}	5×10^{11}	1×10^{-31}	9×10^{17}

The doped zinc blende GaN is used, because the effective mass there is smaller than in wurtzite GaN, whereas another parameters are almost the same.

The typical results of dependencies of the increments of instability on the longitudinal wave number $\omega''(k) > 0$ are presented in **Figures 2-5**. In the structures graphene-semiconductor the increments are $\omega''(k) > 10^{12}$ s^{-1} under moderate values of the drift velocities $v_0 \approx (0.3 \div 0.6) v_F$ and under the electron temperatures $T \leq 200$ K. 2D electron concentration in graphene should be high, $n_{20} \geq 5 \times 10^{11}$ cm^{-2}. In the doped semiconductors there is a possibility not only to control the frequency of the SCW, but also to increase the increment of instability. The amplification can occur both in polar semiconductors like GaAs, GaN, InN, and in doped

non-polar ones like n-Si. The resonant frequencies are in THz range, $\omega' = 3 \times 10^{13}$ $s^{-1} \div 1.5 \times 10^{14}$ s^{-1}; they depend weakly on the electron temperature T and on the drift velocity v_0.

In Figure 2 the results of simulations are presented for non-polar semiconductor n-Si. Under realistic values of electron concentration the increments of instability are moderate and reach the values of $\omega'' = 7 \times 10^{11}$ s^{-1}. In non-polar semiconductors namely the interaction of 2D electronic drift with the electron plasma results in the instability of the hybrid waves. The instability occurs at THz frequencies of about $\omega' = 3 \times 10^{13}$ s^{-1}.



(a) (b)

Figure 2. The case of non-polar doped semiconductor n-Si, $\varepsilon(0) = 11.9 = \varepsilon_\infty$, the electron effective mass is $m_V^* = 2 \times 10^{-31}$ kg. The electron temperature is $T = 80$ K, the drift velocity is $v_0 = 0.6 v_F$, the electron collison frequency in graphene is $\nu_p = 2 \times 10^{12}$ s^{-1}. Part a) is the dependencies of the real part of the frequency $\omega'(k)$ under instability of hybrid SCW, part b) is the dependencies of the increment of instability $\omega''(k)$. Curves 1 are for the 3D electron concentration $n_0 = 5 \times 10^{17}$ cm^{-3}, the bulk collison frequency $\gamma_2 = 2.5 \times 10^{12}$ s^{-1}; curves 2 are for $n_0 = 1 \times 10^{18}$ cm^{-3}, $\gamma_2 = 3 \times 10^{12}$ s^{-1}; curves 3 are for $n_0 = 1.5 \times 10^{18}$ cm^{-3}, $\gamma_2 = 4 \times 10^{12}$ s^{-1}.

In Figures 3-5 the results are given for the polar semiconductors GaAs, GaN, and InN. The comparison with the instability in heterotructures GaAs-$Ga_{1-x}Al_xAs$, GaN-$Ga_{1-x}Al_xN$, and InN-$In_{1-x}Al_xN$ is realized, curves 1 there. As our simulations have demonstrated, the increments of instability in the structures on the base of narrow-gap semiconductors InSb, InAs are smaller than ones presented in Figures 3-5, despite very small electron masses there.

In Figure 3 there are simulations for GaAs. It is seen that in undoped i-GaAs the increment of instability is even smaller than in n-Si. But in doped n-GaAs the increment is comparable. The instability occurs at the drift velocities $v_0 \geq 0.5 v_F$. Therefore, when using GaAs, it is better to apply the doped semiconductors. The inctements of instability in the heterostructure is a bit higher than in the structure graphene-n-GaAs. The frequencies of the hybrid waves are of about $\omega' = 5.5 \times 10^{13}$ s^{-1}.

Essentially higher inctements have been obtained with the nitrides GaN, InN. In Figure 4 the results of simuations are presented for zinc blende GaN. The increments of instability are essentially higher then in n-GaAs and may reach the

values of 2.5×10^{12} s^{-1}. In the doped n-GaN increments can be 30% increased when compared with i-GaN. The instability occurs at the drift velocities in graphene $v_0 \geq 0.4 v_F$. Frequencies are higher than in n-GaAs, they are about $\omega' = 1.4 \times 10^{14}$ s^{-1}. For the structures with wurtzite GaN, the use of doping does not increase the increments.

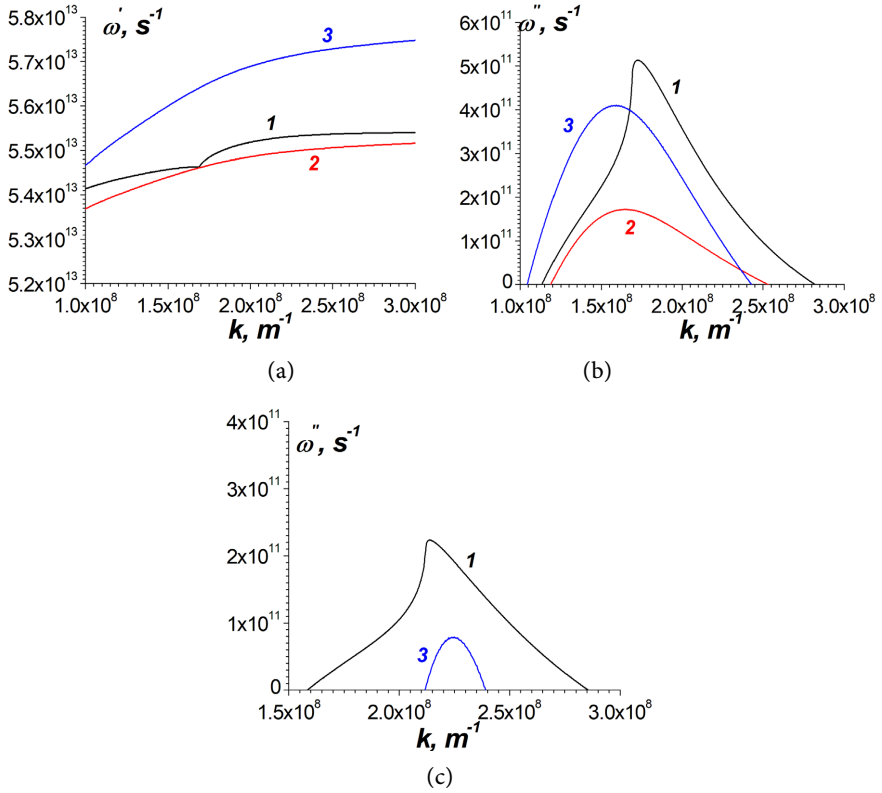
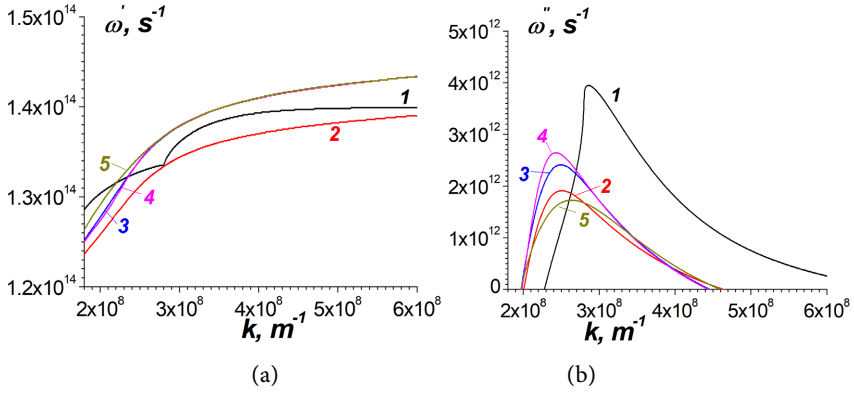
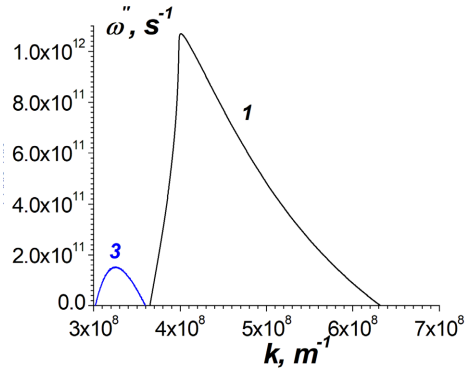


Figure 3. The case of polar semiconductor GaAs; $\varepsilon(0) = 12.9$, $\varepsilon_\infty = 10.9$, the effective mass is $m_V^* = 6 \times 10^{-32}$ kg, the electron temperature is $T = 80$ K. Part a) is the dependencies of the real part of the frequency $\omega'(k)$ under instability of hybrid SCW, $v_0 = 0.6 v_F$; part b) is the dependencies of the increment of instability $\omega''(k)$, $v_0 = 0.6 v_F$, part c) is the dependencies of the increment of instability $\omega''(k)$, $v_0 = 0.5 v_F$. Curves 1 are for the heterostructure on the base of GaAs; the collision frequency of 2D electron gas is $\nu_p = 1 \times 10^{11}$ s^{-1}. Curves 2 are for the structure with graphene, undoped semiconductor i-GaAs. Curves 3 are for the structure with graphene, the doped n-GaAs, $n_0 = 3 \times 10^{17}$ cm^{-3}, $\gamma_2 = 7 \times 10^{12}$ s^{-1}.



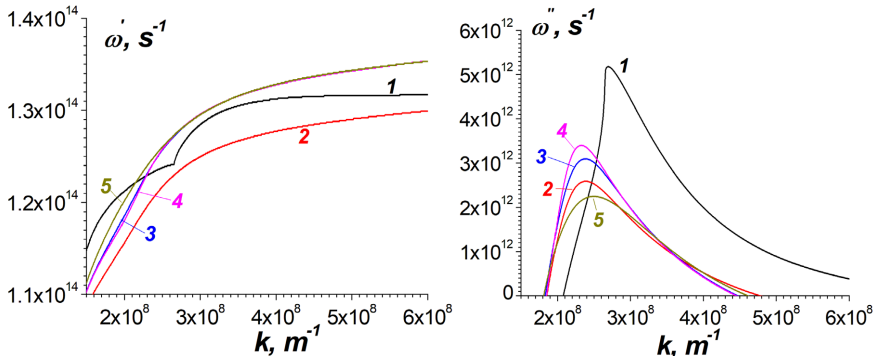


(c)

Figure 4. The case of polar semiconductor GaN; $\varepsilon(0)$ =9.7, ε_∞ = 5.3, the effective mass is m_V^* = 1×10^{-31} kg. Part a) is the dependencies of the real part of the frequency $\omega'(k)$ under instability of hybrid SCW, $v_0 = 0.6 v_F$; part b) is the dependencies of the increment of instability $\omega''(k)$, $v_0 = 0.6 v_F$, part c) is the dependencies of the increment of instability $\omega''(k)$, $v_0 = 0.4 v_F$. Curves 1 are for the heterostructure on the base of GaN, the collision frequency of 2D electron gas is $\nu_p = 1 \times 10^{11}$ s^{-1}. Curves 2-5 are for the structure with graphene. Curves 2 are for the undoped semiconductor *i*-GaN, T = 80 K. Curves 3 are for the doped *n*-GaN, $n_0 = 5 \times 10^{17}$ cm^{-3}, $\gamma_2 = 1 \times 10^{13}$ s^{-1}, T = 80 K. Curves 4, 5 are the same as 3, but the electron temperatures are T = 50 K and T = 200 K, correspondingly.

The highest increments of instability have been obtained in the structures on the base of semiconductor InN, as shown in Figure 5. The doping increases increments unessentially, compare curves 2 and 3 in Figure 5, part b. The instability occurs at the drift velocities $v_0 \geq 0.3 v_F$. The circular frequencies of hybrid waves are about ω' =1.3×10^{14} s^{-1}. Doping of GaN and InN may control these frequencies.

In nitrides GaN, InN the instability can be in a wide temperature range, at relatively low drift velocities. Doping increases the increments inessentially. Therefore, it is simpler to use undoped semiconductors. Generally, increments are slightly higher in heterostructures than in graphene, but they are comparable. Because the fabrication of structures with graphene is simpler and more flexible, they seem perspective for observing such instability. Thus, the efficiency of instability is determined by the ratio $(\varepsilon(0) - \varepsilon_\infty)/\varepsilon(0)$, which is the highest in the semiconductor InN.



(a) (b)

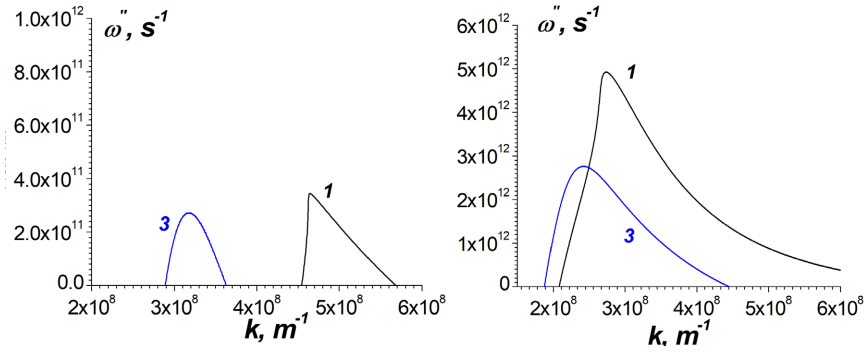


Figure 5. The case of polar semiconductor InN; $\varepsilon(0)$ =14.0, ε_∞ = 5.8, the effective mass is m_V^* = 1×10^{-31} kg. Part a) is the dependencies of the real part of the frequency $\omega'(k)$ under instability of hybrid waves, $\nu_0 = 0.6\nu_F$; part b) is the dependencies of the increment of instability $\omega''(k)$, $\nu_0 = 0.6\nu_F$, part c) is the dependencies of the increment of instability $\omega''(k)$, $\nu_0 = 0.3\nu_F$; part d) is for the increased values of the collision frequency in graphene $\nu_p = 5 \times 10^{12}$ s^{-1}, $\nu_0 = 0.6\nu_F$. Curves 1 are for the heterostructure on the base of InN, the collision frequency of 2D electron gas is $\nu_p = 1 \times 10^{11}$ s^{-1}. Curves 2-5 are for the structure with graphene. Curves 2 are for undoped semiconductor *i*-InN, T = 80 K. Curves 3 are for the doped *n*-InN, $n_0 = 5 \times 10^{17}$ cm^{-3}, $\gamma_2 = 1 \times 10^{13}$ s^{-1}, T = 80 K. Curves 4, 5 are the same as 3, but the electron temperatures are T = 50 K and T = 200 K, correspondingly.

The amplification coefficient in the longitudinal direction x can be estimated for semiconductor InN as $k'' \approx \omega''/v_0 \approx 5 \times 10^6$ m^{-1}, for $\omega'' = 3 \times 10^{12}$ s^{-1}, $v_0 = 0.6 \times 10^8$ cm/s. Thus, the length of the structure along OX axis should be about $L_x \approx 4$ μm, to provide the amplification $\exp(k''\cdot L_x) \approx 10^8$. To realize the generation of hybrid SCW, it is necessary to create additional positive feedback when the part of the output energy of the amplified hybrid wave is transferred to the input of the system.

The maximum increments of instability occur at the wave numbers $k \sim 10^8$ m^{-1}, therefore the transverse size along OZ axis should be of about $L_z \geq 10/k \sim 0.1$ μm for a localization in the transverse direction. The transverse size in the plane along OY axis can be estimated from the relation $L_x/\left(kL_y^2\right) < 10^{-2}$, or $L_y > 3$ μm, *i.e.* when the role of wave diffraction is unessential.

In this paper only the linear problem of instability or amplification is considered. The nonlinearity may result in decreasing drift velocity and increasing electron temperature in graphene. Because the instability of hybrid waves and their amplification occur in wide intervals of electron temperatures and drift velocities, the structures on the base of graphene possess a preference over the quantum structures with GaN, InN with respect to the influence of the nonlinearity. As our earlier simulations demonstrated [11], the increments of instability decreased in the heterostructures at the electron temperatures $T \geq 120$ K.

Here the kinetic approach both for structures with graphene and for heterostructures has been applied. Also, the hydrodynamic approach can be applied to investigate the drift instability. As our simulations have demonstrated, the hydrodynamic approach yields similar results for the increments of the drift instability. For graphene the increments, which are simulated from the hydrodynamic ap-

proach, are a bit smaller than ones from the kinetic approach, whereas for heterostructures they are overestimated [12] [13].

4. Discussion

Structures graphene-nitride semiconductors are characterized by high increments of drift instability and high amplification coefficients of the hybrid space charge waves in graphene-optical phonons and plasmons in semiconductors. With graphene, it is easy to get high drift velocities of 2D electron gas. The preference is a simpler fabrication, compared to heterostructures with selective doping. The lack is relatively high collision frequencies in graphene.

In the heterostructures with 2D electron gas in quantum wells on the base of nitrides there are high increments of the instability and low collision frequencies. Due to the last factor, the increments may be somewhat higher than in the structures with graphene. But the problem is more complex fabrication of heterostructures with quantum wells. The temperature interval, which may be used to observe the instability, is wider in the structures with graphene.

For experimental realization, it is simpler to use the intrinsic semiconductors *i*-GaN, *i*-InN, because the interaction with electron plasmons does not result in essential increase of increments. The amplification of hybrid waves should be realized in the pulse regime, to prevent heating the structures.

5. Conclusions

The structures graphene-semiconductor layers can be used for generation and amplification of hybrid space charge waves in graphene-optical phonons or plasmons in semiconductors in terahertz range. The mechanism of amplification is based on the Cherenkov effect under the drift of two-dimensional electron gas in graphene. The velocity of electron drift should exceed the phase velocity of the hybrid wave. The results of computer simulations for realistic parameters of graphene and semiconductor layers show the possibility of observing the specified instability. The best results have been obtained by using nitride semiconductors GaN, InN. The increments of instability may reach the values of 3×10^{12} s^{-1} when the drift velocity is $v_0 = 6 \times 10^7$ cm/s. These increments are satisfactory for the practical realization. In doped *n*-InN the increment of instability increases unessentially, so for experimental realization it is possible to use intrinsic semiconductors. But by means of doping levels in semiconductors, it is possible to control the resonant frequency of hybrid waves for the realization of instability. The cooling of structures temperatures should be moderate with temperatures of about $T \sim 100$ K.

The quantum kinetic approach has been used to investigate this instability. The hydrodynamic approach for 2D electron dynamics also can be applied, but only for rough estimations of increments of instability.

The simulated increments of instability in the heterostructures on the base of GaN, InN are comparable with ones simulated for the structures graphene-nitride

semiconductors. But the structures with graphene seem more perspective when compared to the semiconductor quantum heterostructures on the base of GaN, InN, because of easier fabrication and wider temperature intervals for observing instability.

Acknowledgements

Yuriy Rapoport acknowledges the National Science Centre, Poland, for funding initiative under project number UMO-2023/49/B/ST10/03465. Volodymyr Grimalsky, Margarita Tecpoyotl-Torres, and Oskar Nava-Fuerte are grateful to SEP-CONAHCyT (Mexico) for partial funding.

Author Contributions

Conceptualization, V.G. and Y.R.; methodology, V.G. and M.T.; software, V.G. and O.N.; validation, V.G., Y.R., and M.T.; formal analysis, Y.R. and M.T.; investigation, V.G and Y.R.; resources, O.N.; data curation, V.G.; writing—original draft preparation, V.G. and O.N.; writing—review and editing, V.G.; visualization, V.G. and O.N.; supervision, V.G. and M.T.; project administration, M.T.; funding acquisition, V.G. and M.T.

Conflicts of Interest

The authors declare no conflicts of interest regarding the publication of this paper.

References

[1] Siegel, P.H. (2002) Terahertz Technology. *IEEE Transactions on Microwave Theory and Techniques*, **50**, 910-928. https://doi.org/10.1109/22.989974

[2] Perenzoni, M. and Paul, D.J. (2014) Physics and Applications of Terahertz Radiation. Springer.

[3] Biswas, A., Banerjee, A., Acharyya, A., Inokawa, H. and Nath Roy, J. (2020) Emerging Trends in Terahertz Solid-State Physics and Devices Sources, Detectors, Advanced Materials, and Light-Matter Interactions. Springer.

[4] Bründermann, E., Hübers, H.W. and Kimmitt, M.F. (2012) Terahertz Techniques. Springer.

[5] Carpintero, G., Garcıa Muñoz, L.E., Hartnage, L.H.L., Preu, S. and Räisänen, A.V. (2015) Semiconductor Terahertz Technology Devices and Systems at Room Temperature Operation. Wiley.

[6] Dexheimer, S.L. (2008) Terahertz Spectroscopy Principles and Applications. CRC Press.

[7] Ward, J.S., Chattopadhyay, G., Gill, J., Javadi, H., Lee, C., Lin, R., *et al.* (2008) Tunable Broadband Frequency-Multiplied Terahertz Sources. 2008 33*rd International Conference on Infrared, Millimeter and Terahertz Waves*, Pasadena, 15-19 September 2008, 1-3. https://doi.org/10.1109/icimw.2008.4665437

[8] Rieh, J.-S. (2021) Introduction to Terahertz Electronics. Springer.

[9] Yun-Shik, L. (2009) Principles of Terahertz Science and Technology. Springer.

[10] Sze, S.M., Li, Y.M. and Ng, K.K. (2021) Physics of Semiconductor Devices. Wiley.

[11] Castrejon-M., C., Grimalsky, V. and Koshevaya, S. (2012) Amplification of Optical Phonons in Bulk Semiconductors and Heterostrutures at Low Temperatures. 2012 28*th International Conference on Microelectronics Proceedings*, Nis, 13-16 May 2012, 277-280. https://doi.org/10.1109/miel.2012.6222853

[12] Castrejon-M, C., Grimalsky, V.V., Koshevaya, S.V. and Tecpoyotl-T, M. (2014) Amplification of Optical Phonons in Narrow Band Semiconductors at Low Temperatures. *Radioelectronics and Communications Systems*, **57**, 70-77. https://doi.org/10.3103/s0735272714020022

[13] Grimalsky, V., Tecpoyotl-Torres, M., Rapoport, Y. and Nava-Fuerte, O. (2025) Amplification of Terahertz Optical Phonons and Plasmons in the Structures Graphene-Semiconductor by 2D Electron Drift. 2025 *IEEE* 34*th International Conference on Microelectronics* (*MIEL*), Nis, 13-16 October 2025, 1-4. https://doi.org/10.1109/miel66332.2025.11261039

[14] Su, Z.X., Xiong, B., Xu, Y.H., Cai, Z.Q., *et al.* (2019) Manipulating Cherenkov Radiation and Smith-Purcell Radiation by Artificial Structures. *Advanced Optical Materials*, **14**, Article 1801666. https://doi.org/10.1002/adom.201801666

[15] Kondrat'ev, A.S. and Kuchma, A.E. (1989) Lectures on the Theory of Quantum Liquids (Lektsii po Teorii Kvantovykh Zhidkostey, in Russ.). St. Petersburg University Press.

[16] Lifshitz, E.M. and Pitaevskii, L.P. (1981) Physical Kinetics. Pergamon.

[17] Grimalsky, V., Rapoport, Y., Koshevaya, S., Nosich, A. and Escobedo-Alatorre, J. (2025) Linear and Nonlinear Resonant Properties of Electron Gas in N-InSb and Graphene Layers in Terahertz Range in Bias Magnetic Fields. *Materials Research Express*, **12**, Article 016102. https://doi.org/10.1088/2053-1591/ada5b7

[18] Datta, S. (1999) Electronic Transport in Mesoscopic Systems. Cambridge University Press.

[19] Levitov, L. and Falkovich, G. (2016) Electron Viscosity, Current Vortices and Negative Nonlocal Resistance in Graphene. *Nature Physics*, **12**, 672-676. https://doi.org/10.1038/nphys3667

[20] Krishna Kumar, R., Bandurin, D.A., Pellegrino, F.M.D., Cao, Y., Principi, A., Guo, H., *et al.* (2017) Superballistic Flow of Viscous Electron Fluid through Graphene Constrictions. *Nature Physics*, **13**, 1182-1185. https://doi.org/10.1038/nphys4240

[21] Bandurin, D.A., Shytov, A.V., Levitov, L.S., Kumar, R.K., Berdyugin, A.I., Ben Shalom, M., *et al.* (2018) Fluidity Onset in Graphene. *Nature Communications*, **9**, Article No. 4533. https://doi.org/10.1038/s41467-018-07004-4

[22] Katsnelson, M.I. (2020) The Physics of Graphene. 2nd Edition, Cambridge University Press. https://doi.org/10.1017/9781108617567

[23] Shafraniuk, S. (2015) Graphene. Fundamentals, Devices, and Applications. CRC Press.

[24] Stoer, J. and Bulirsch, R. (1996) Introduction to Numerical Analysis. Springer.

[25] Yu, P.Y. and Cardona, M. (2010) Fundamentals of Semiconductors. Springer.

[26] Levinshtein, M., Rumyantsev, S. and Shur, M. (1999) Handbook Series on Semiconductor Parameters 1. World Scientific Publishing.